Differential Incision of Bulky Carcinogen−DNA Adducts by the UvrABC Nuclease: Comparison of Incision Rates and the Interactions of Uvr Subunits with Lesions of Different Structures†

Sarasija Hoare,‡,# Yue Zou,‡ Vandana Purohit,§ Ramji Krishnasamy,§ Milan Skorvaga,|| Bennett Van Houten,*,|| Nicholas E. Geacintov,⊥ and Ashis K. Basu*,§

Department of Chemistry, University of Connecticut, Box U-60, Storrs, Connecticut 06269

Received June 8, 2000; Revised Manuscript Received August 11, 2000

ABSTRACT: The UvrABC nuclease system from *Escherichia coli* removes DNA damages induced by a wide range of chemical carcinogens with variable efficiencies. The interactions with UvrABC proteins of the following three lesions site-specifically positioned in DNA, and of known conformations, were investigated: (i) adducts derived from the binding of the (−)-(7*S*,8*R*,9*R*,10*S*) enantiomer of 7,8-dihydroxy-9,10-epoxy-7,8,9,10-tetrahydrobenzo[*a*]pyrene [(−)-*anti*-BPDE] by *cis*-covalent addition to N^2-2′-deoxyguanosine [(−)-*cis*-*anti*-BP-N^2-dG], (ii) an adduct derived from the binding of the (+)-(1*R*,2*S*,3*S*,4*R*) enantiomer of 1,2-dihydroxy-3,4-epoxy-1,2,3,4-tetrahydro-5-methylchrysene [(+)-*anti*-5-MeCDE] by trans addition to N^2-2′-deoxyguanosine [(+)-*trans*-*anti*-MC-N^2-dG], and (iii) a C8-2′-deoxyguanosine adduct (C8-AP-dG) formed by reductively activated 1-nitropyrene (1-NP). The influence of these three different adducts on UvrA binding affinities, formation of UvrB−DNA complexes by quantitative gel mobility shift analyses, and the rates of UvrABC incision were investigated. The binding affinities of UvrA varied among the three adducts. UvrA bound to the DNA adduct (+)-*trans*-*anti*-MC-N^2-dG with the highest affinity ($K_d = 17 \pm 2$ nM) and to the DNA containing C8-AP-dG with the least affinity ($K_d = 28 \pm 1$ nM). The extent of complex formation with UvrB was also the lowest with the C8-AP-dG adduct. 5′ Incisions occurred at the eighth phosphate from the modified guanine. The major 3′ incision site corresponded to the fifth phosphodiester bond for all three adducts. However, additional 3′ incisions were observed at the fourth and sixth phosphates in the case of the C8-AP-dG adduct, whereas in the case of the (−)-*cis*-*anti*-BP-N^2-dG and (+)-*trans*-*anti*-MC-N^2-dG lesions additional 3′ cleavage occurred at the sixth and seventh phosphodiester bonds. Both the initial rate and the extent of 5′ and 3′ incisions revealed that C8-AP-dG was repaired less efficiently in comparison to the (−)-*cis*-*anti*-BP-N^2-dG and (+)-*trans*-*anti*-MC-N^2-dG containing DNA adducts. Our study showed that UvrA recognizes conformational changes induced by structurally different lesions and that in certain cases the binding affinities of UvrA and UvrB can be correlated with the incision rates. The size of the bubble formed around the damaged site with mismatched bases also appears to influence the incision rates. A particularly noteworthy finding in this study is that UvrABC repair of a substrate with no base opposite C8-AP-dG was quite inefficient as compared to the same adduct with a C opposite it. These findings are discussed in terms of the available NMR solution structures.

Nucleotide excision repair (NER)[1] ensures the fidelity of replication by the removal of a wide range of carcinogen−DNA adducts and UV light-induced photoproducts formed in DNA (*1*−*3*). In *Escherichia coli* UvrABC endonucleases recognize and initiate the elimination of different adducts by the incision of a damaged strand containing the modified

†This work was supported by NIH Grants ES09127 to A.K.B., CA76660 to N.E.G., and ES07955 to B.V.H., and a NIEHS Center Grant ES06676 to R. Stephen Lloyd. A.K.B. is a recipient of a Research Career Development Award (K02ES00318) from NIEHS.

* To whom all correspondence should be addressed: (A.K.B.) Department of Chemistry, University of Connecticut, Storrs, CT 06269. Telephone: 860-486-3965. Fax: 860-486-2981. E-mail: akbasu@nucleus.chem.uconn.edu. (B.V.H.) Laboratory of Molecular Genetics, NIEHS, Research Triangle Park, NC 27709. Telephone: 919-541-7752. E-mail: vanhout1@niehs.nih.gov.

‡Sealy Center for Molecular Science, University of Texas Medical Branch, Galveston, TX, 77555.

§ Department of Chemistry, University of Connecticut, Storrs, CT 06269.

|| Laboratory of Molecular Genetics, National Institute of Environmental Health Sciences, National Institutes of Health, Research Triangle Park, NC 27709.

⊥ Department of Chemistry, New York University, New York, NY 10003.

Current Address for Dr. Sarasija Hoare: Shands Cancer Center, University of Florida, P.O. Box 10032, Gainesville, FL 32610.

[1] Abbreviations: NER, nucleotide excision repair; PAH, polycyclic aromatic hydrocarbon; BPDE, 7,8-dihydroxy-9,10-epoxy-7,8,9,10-tetrahydrobenzo[*a*]pyrene; 5-MeCDE, 1,2-dihydroxy-3,4-epoxy-1,2,3,4-tetrahydro-5-methylchrysene; 1-NP, 1-nitropyrene; C8-AP-dG, *N*-(deoxyguanosin-8-yl)-1-aminopyrene; (−)-*cis*-*anti*-BP-N^2-dG, adduct derived from the cis addition of the (−)-7*S*,8*R*,9*R*,10*S* stereoisomer of BPDE [(−)-*anti*-BPDE] to the exocyclic amino group of 2′-deoxyguanosine; (+)-*trans*-*anti*-MC-N^2-dG, adduct derived from the trans addition of the 1*R*,2*S*,3*S*,4*R* stereoisomer of 5-MeCDE [(+)-anti-5-MeCDE] to the exocyclic amino group of 2′-deoxyguanosine.

10.1021/bi0013187 CCC: $19.00
Published on Web 09/15/2000

nucleotide as a dodecamer (*4*). This dual-incision mechanism, where the enzyme acts at a distance from the adducted site, might explain the broad substrate specificity of the enzyme (*5*). However, the nature of protein−DNA interactions between the repair subunits and the damaged site, which might determine the efficiency of incision, has not been clearly elucidated. Lesions embedded in different sequences are repaired at different rates, and no consensus DNA sequence has been found for maximum binding of damage recognition proteins (*6*, *7*). Various types of DNA lesions are removed at very different rates. The dynamic conformation of the adducted site influenced by the chemical structure of the lesion, which varies with the DNA sequence context, is likely to influence damage recognition and repair efficiency (*8*−*12*). UvrABC endonuclease, a multienzyme complex containing three subunits, UvrA, UvrB, and UvrC acts in a sequential manner on the damaged site to excise a broad spectrum of lesions with high specificity (*13*, *14*). UvrA plays an important role in damage recognition (*15*). UvrA dimerizes in solution and interacts with UvrB, resulting in the formation of a heterodimer $UvrA_2B$ (*16*, *17*). The $UvrA_2B$ complex binds to the DNA duplex and translocates along the DNA to the lesion using the 5′ to 3′ helicase activity of this complex (*18*, *19*). The DNA in this complex is subjected to unwinding, kinking, and bending (*20*). Dissociation of UvrA follows the formation of a stable UvrB−DNA complex that is locally denatured by 5−6 base pairs around the lesion and bent by 130° (*21*, *22*). The size and hydrophobicity of the lesion, which probably interacts with a hydrophobic pocket in UvrB, contribute to the ability of the lesion to function as a substrate for UvrB (*23*). Interaction of UvrB with UvrC triggers incision at the fourth to seventh phophodiester bond 3′ to the modified base (*24*, *25*), which is rapidly followed by incision at the eighth phosphodiester bond 5′ to the damaged base (*2*). Recent site-directed mutagenesis studies (*26*) indicate that, in contrast to the previous reports (*24*), the N-terminal portion of UvrC is responsible for 3′ incision and the C-terminal portion of UvrC is responsible for 5′ incision.

A long-term challenge in understanding protein−DNA interactions involved in damage recognition is to correlate apparent binding affinities of DNA repair proteins to known structural alterations. Even though UvrA is viewed as the primary damage recognition subunit, a direct correlation between incision rate and UvrA binding efficiency is not always found (*15*, *25*, *27*). UvrB, known as the specificity subunit, plays a central role in the excision reaction because it interacts with all the components in damage repair including modified DNA, UvrA, UvrC, and DNA polymerase I (*13*, *28*). Our major goal is to investigate whether UvrA and UvrB can recognize conformational changes induced by various bulky lesions and also to establish a relationship of the binding affinity of the UvrA and UvrB proteins with the rates of repair. In the current study, we examined in detail, the interaction of UvrA and UvrB proteins and incision efficiency of the UvrABC nuclease system with three structurally well-characterized DNA adducts. The first is formed from the reaction of 1-nitropyrene (1-NP) to C8-dG (*29*, *30*). The second adduct results from the binding by *cis*-addition to N^2-dG of the (+)-(1*R*,2*S*,3*S*,4*R*) enantiomer of 1,2-dihydroxy-3,4-epoxy-1,2,3,4-tetrahydro-5-methylchrysene [(+)-*anti*-5-MeCDE], resulting in the (+)-*trans*-*anti*-MC-N^2-dG adduct (*31*). The third adduct has been isolated from the reaction of the (−)-(7*S*,8*R*,9*R*,10*S*) enantiomer of 7,8-dihydroxy-9,10-epoxy-7,8,9,10-tetrahydrobenzo[*a*]pyrene [(−)-*anti*-BPDE] by cis addition to N^2-dG to form the (−)-*cis*-*anti*-BP-N^2-dG adduct (*32*).

We examined the interaction of UvrABC nucleases with 50-mer substrates containing, at the identical site of a defined sequence, one of the three lesions, the C8-AP-dG, the (−)-*cis*-*anti*-BP-N^2-dG or the (+)-*trans*-*anti*-5-MC-N^2-dG adduct. We determined the binding affinities of UvrA to these lesions, characterized the UvrB-DNA preincision complex by quantitative gel mobility analysis, and determined the efficiencies of incision results on the 5′ and 3′ sides of the lesions. While the interactions of the different stereoisomeric *anti*-BP-N^2-dG lesions with UvrABC proteins have been reported (*25*), the (−)-cis-*anti*-BP-N^2-dG lesion is used here for comparison with the results obtained with the C8-AP-dG and the (+)-*trans*-*anti*-5-MC-N^2-dG adduct. This is the first study that shows that the (+)-*trans*-*anti*-MC-N^2-dG adduct is one of the lesions that are efficiently recognized and incised by UvrABC. Our studies also indicated that C8-AP-dG is recognized but repaired less efficiently in comparison with the (−)-*cis*-*anti*-BP-N^2-dG and (+)-*trans*-*anti*-MC-N^2-dG adducts. The size of the denatured region around the site of the lesion influences the rate of repair. In addition, we have shown that, when the cytosine opposite C8-AP-dG is absent [modeling the promutagenic deletion intermediates that result in an increased thermodynamic stability of the DNA duplex (*33*)], the incision rate is reduced by half.

MATERIALS AND METHODS

Materials. Acrylamide, ammonium persulfate, *N*,*N*′-methylenebisacrylamide, and urea were purchased from Bethesda Research Laboratories, Gaithersberg, MD. [γ^{32}P] ATP and [α^{32}P] cordycepin-5′-triphosphate were purchased from New England Nuclear, Boston, MA. The racemic BPDE was purchased from the National Cancer Institute Chemical Carcinogen Reference Repository, Bethesda, MD. The racemic (±) *anti* 5-MeCDE was a kind gift from Dr. S. Amin and was synthesized following published procedures (*34*). 1-NP and 1-aminopyrene were obtained from Aldrich Chemical Co., Milwaukee, WI. All restriction and modification enzymes were purchased from Promega (Madison, WI) or New England Biolabs (Beverly, MA) unless otherwise indicated.

DNA Sequence Analysis. DNA sequencing was performed using a cycle sequencing protocol using Ampli Taq DNA polymerase (Perkin-Elmer Corp., Norwalk, CT). Sequence analysis was performed using a model 373A DNA sequence analyzer (Perkin-Elmer Applied Biosystems, Foster City, CA).

Estimation of Protein Concentrations. The protein concentrations were determined by the Bio-Rad protein assay kit, using bovine serum albumin as a standard, following the manufacturer's instructions.

Purification of UvrA, UvrB, and UvrC Proteins. (a) UvrA. UvrA was purified to homogeneity as described earlier (*25*) from *E. coli* strain MH1 ΔuvrA containing the overproducing plasmid, pSST10 (kindly supplied by L. Grossman, Johns Hopkins University), which is under the control of the heat-inducible PL promoter.

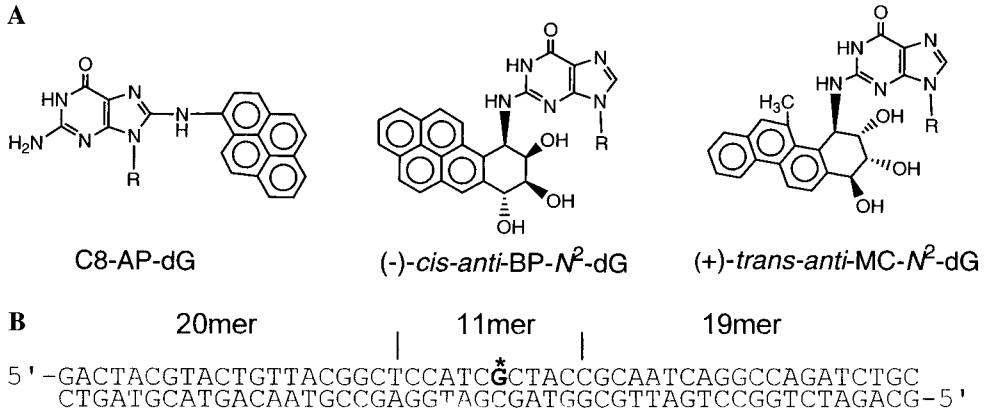

FIGURE 1: Panel A: Structures of C8-AP-dG, (−)-*cis-anti*-BP-N^2-dG, and (+)-*trans-anti*-MC-N^2-dG. Panel B: Construction of adducted 50-mer DNA substrate. The bold G with the asterisk in the sequence represents the modified base. Construction of the 50-mer has been described in Materials and Methods.

(b) UvrB. UvrB, cloned in pCYB2 of the Impact system, New England Biolabs, under the control of the IPTG-inducible P_{tac} promoter was overexpressed in XL-1 Blue and purified in a single step using a chitin column as described (*22*).

(c) UvrC. Single step purification of UvrC was achieved by subcloning PCR amplified uvrC with *Nde*1 and *Kpn*1 ends in pTYB1 overexpression plasmid (T7 Impact system, NEB) in-frame to the splice protein intein and chitin binding domain under the T7 promoter. The entire sequence of UvrC was verified after subcloning in the Impact system. The recombinant plasmid was transformed in *E. coli* C41 (DE3). This mutant host strain can grow to high saturation cell density and can produce the protein as inclusion bodies at an elevated level without toxic effect (*35*). C41 (DE3) containing pTYB1UvrC were grown at 25 °C, and IPTG was added to a final concentration of 1 mM, when A_{600} reached 0.5, cells were harvested (∼3 h). Cell pellets from 1 L of culture were suspended in 20 mL of cell lysis buffer (20 mM Tris-HCl, pH 8.0, 500 mM NaCl, 0.1 mM EDTA, and 0.1% Triton X-100) and sonicated to lyse the cells completely, and the clear lysate was loaded onto a chitin column (3 mL) equilibrated with the cell lysis buffer. The column was washed with 30 vol of the equilibration buffer. The on-column cleavage of UvrC protein from the intein−chitin fusion protein was induced by flushing the column quickly with 3 column vol of the cleavage buffer (20 mM Tris-HCl, pH 8.0, 100 mM NaCl, 0.1 mM EDTA, and 30 mM DTT), and the column was closed immediately. The cleavage was allowed to continue overnight at 4 °C. UvrC was eluted from the column with cleavage buffer without DTT and dialyzed against the storage buffer (50 mM Tris-HCl, pH 7.8, 100 mM KCl, 0.1 mM EDTA, 1 mM DTT, and 50% glycerol). Analysis of UvrC preparation on SDS−PAGE gel followed by Coomassie blue staining showed a single band. The incision activity of UvrC purified by the Impact system was comparable to the UvrC directly purified from the plasmid pDR3274 as described by Sancar et al. (*36*) (data not shown).

The enzymes were stored at −80 °C in storage buffer containing 50 mM Tris-HCl, pH 7.5, 100 mM KCl, 1 mM EDTA, 1mM DTT, and 50% glycerol.

Preparation of 50-mer DNA Duplexes Containing the Lesion. All the unmodified oligonucleotides were synthesized on an Applied BioSystems 394DNA/RNA synthesizer. Oligonucleotides were purified by polyacrylamide gel electrophoresis under denaturing conditions. The 11-mers [d(CCATC[G*]CTACC)] containing the adducts [G*] = (−)-*cis-anti*-BP-N^2-dG, (+)-*trans-anti*-5-MC-N^2-dG, and C8-AP-dG were synthesized, purified, and characterized as described earlier (*31*, *32*, *37*). The 50-mer substrates were prepared by ligating equimolar amounts of 20-mer, adducted 11-mer, and 19-mer (appropriately 5′-phosphorylated) in the presence of a 50-mer complementary strand (bottom strand in Figure 1, panel B). Thirty picomoles of 20-mers were mixed with equal amounts of the 11-mers, 19-mers (phosphorylated with nonradiolabeled ATP), and 30 pmol of the bottom strand in 30 μL reaction mixtures containing 50 mM Tris-HCl, pH 7.8, 10 mM $MgCl_2$, 10 mM DTT, 1 mM ATP, and 50 μg/mL BSA. The oligomers were annealed to the bottom strand by heating the reaction mixture at 80 °C for 5 min and allowing it to cool slowly to room temperature and finally to 16 °C. One unit of T4 DNA ligase was added, and the incubation was continued at 16 °C for 18 h. The samples were heated at 80 °C for 5 min in the presence of 8 M urea and loaded onto a 12% (w/v) denaturing polyacrylamide gel. The band corresponding to the 50-mer was cut out, and the DNA was eluted by crush/soak procedure in a buffer containing 0.5 M ammonium acetate, 10 mM magnesium acetate, and 1 mM EDTA and then was precipitated with ethanol. The 50-mers were resuspended in 30 μL of annealing buffer (10 mM Tris-HCl, pH 8.0, 100 mM NaCl, 1 mM EDTA) along with 30 pmol of the complementary bottom strand, and annealing was carried out by heating at 80 °C for 5 min followed by cooling slowly to room temperature. Excess single-stranded DNA was removed by running the samples on a 10% nondenaturing polyacrylamide gel. The 50-mer duplexes were cut out and purified by crush/soak method. The concentration of the DNA was determined using the molar extinction coefficient ϵ_{260} = 660 000 M^{-1} cm^{-1}.

The substrates with partially mismatched bottom strands were prepared by allowing the ligation to take place in the presence of a 55-mer bottom strand containing the complementary sequence of 50 bases and additional five deoxythymidines (dT) residues at the 3′ end. After ligation, the products were purified on an 8% denaturing polyacrylamide gel and reannealed with the 50-mer bottom strands containing three or six nucleotide mismatches or a deletion (Table 3).

To obtain 3′ terminally labeled substrates, the 19-mer (Figure 1, panel B) was labeled at the 3′ end with [α ^{32}P]

cordycepin-5′-triphosphate. Ligation and purification was carried out as described above.

Electrophoretic Mobility Shift Assay. Quantitative estimation of UvrA binding to substrates containing the three adducts was performed by gel shift analysis. End-labeled substrates (1 nM) were incubated with UvrA (5−300 nM) at 37 °C for 15 min in 20-μL reaction mixture containing 50 mM Tris-HCl, pH 7.5, 50 mM KCl, 10 mM $MgCl_2$, 5 mM DTT, and 1 mM ATP. The binding mixtures were analyzed on a 4% native polyacrylamide gel after the addition of 2 μL of 80% glycerol (v/v). The gel was run at 100 V for 2−3 h in TBE buffer (50 mM Tris-HCl, pH 8.0, 50 mM boric acid, 1 mM EDTA) containing 1 mM ATP and 10 mM $MgCl_2$. The gel was dried and exposed to a PhosphorImager screen (Molecular Dyanamics).

The loading of UvrB by UvrA was examined by incubating end-labeled substrates with increasing amounts of UvrA (0−120 nM) in the presence of 200 nM UvrB at 37 °C for 30 min followed by electrophoresis on a 4% polyacrylamide gel as described above.

UvrABC Reactions. UvrABC incubations were carried out at 37 °C with 30 nM UvrA, 80 nM UvrB, 150 nM UvrC, and the DNA substrate (1 nM, 5′ or 3′ terminally labeled) in 40 μL of buffer containing 50 mM Tris-HCl, pH 7.5, 50 mM KCl, 10 mM $MgCl_2$, 5 mM DTT, and 1 mM ATP. The optimal amounts of UvrA, UvrB, and UvrC, which provided the maximum incisions, were determined by using a series of concentrations of the proteins in preliminary experiments. For the time-course studies, the reaction mixture (without UvrC) was brought to 37 °C, before adding UvrC to start the reaction. Aliquots withdrawn at appropriate time points were added to tubes containing EDTA (20 mM) and were heated at 90 °C for 3 min to terminate the reaction. Samples were denatured with formamide loading buffer (50% v/v), heated at 90 °C for 5 min, and analyzed on a 12% polyacrylamide gel under denaturing conditions. The incision products were quantitated in the dried gel.

Quantitative Analysis of Incision and Band Shift Products. Quantitation of incision and band shift results were carried out on a PhosphorImager 425 (Molecular Dynamics) with the aid of IMAGEQUANT software (Molecular Dynamics) using the volume integration method. The amount of DNA incised (DI in fmol) by UvrABC per time point was calculated on the basis of the total molar amount of DNA used in each aliquot (M) and the percentage of radioactivity in the incision products (IP) as compared to the total radioactivity in both the 50-mer and incision products using the formula $DI_{total} = [IP/(50\text{-mer} + IP)]M$.

RESULTS

Construction of the 50-mer DNA Substrates. The interaction of *E. coli* UvrABC with different DNA adducts was studied with 50-mer oligonucleotides carrying the (−)-*cis-anti*-BP-N^2-dG, (+)-*trans-anti*-MC-N^2-dG, or C8-AP-dG lesions (Figure 1, panel A) at the same site in the 50-mer oligonucleotide duplexes (Figure 1, panel B). The substrates were constructed by ligating 11-mers containing the lesion with a 20-mer on the 5′ side and a 19-mer on the 3′ side, after annealing the oligonucleotides on a 50-mer complementary bottom strand. Mild denaturing conditions were employed in the preparation, especially in the case of C8-AP-dG, which was found to be more sensitive to heat and light in comparison to the two PAH adducts. The ligation efficiency of C8-AP-dG was found to be the lowest, whereas unmodified DNA showed the highest efficiency (data not shown). Even though addition of poly(ethylene glycol) (5% v/v) in the ligation reaction improved the yield of the 50-mer products, a corresponding increase in the amount of high molecular weight products was also observed. The ligated and purified 50-mers were reannealed to the complementary strand and the duplexes were gel-purified again to remove excess single-stranded DNA. The homogeneity of the 50-mer duplexes was checked by *Rsa*I restriction enzyme digestion as described previously (*25*).

To construct substrates that contain no base opposite the modified guanine (ΔC) or mismatched sets of bases that form denatured region around the adducted site (bubble), ligation was carried out in the presence of the 55-mer complementary strand. After purification, the adducted 50-mer was annealed to the appropriate bottom strand (Figure 1, panel B).

Damage Recognition by DNA Repair Proteins. (a) Binding of UvrA to Damaged DNA Substrates. UvrA has been shown previously to bind to damaged DNA preferentially (*1*). To investigate the role of UvrA in damage recognition, we performed binding assays with 50-base pair duplexes containing one C8 guanine and two N^2 guanine adducts using gel mobility shift assay and quantitatively analyzed the results. Figure 2 shows the results of a typical mobility shift assay using (+)-*trans-anti*-MC-N^2-dG (1 nM) and UvrA at various concentrations. Gel shift assays were also performed with nondamaged 50-mer and 50-mers containing (−)-*cis-anti*-BP-N^2-dG or C8-AP-dG (data not shown). UvrA forms a $UvrA_2$−DNA complex with a lower mobility (*38*, *39*). Figure 2, panel B, shows a binding isotherm derived from three independent experiments with the (+)-*trans-anti*-MC-N^2-dG adduct-containing DNA. The experimentally determined binding isotherms were best fitted with the model assuming that free UvrA exists predominantly as a dimer in equilibrium with monomers (*15*). The equilibrium dissociation constants ($K_{d,obs}$) were determined from the best-fit of the equations, based on this model, to the experimental data as reported in Zou et al. (*15*).

Table 1 lists the equilibrium dissociation constants for the binding of UvrA to the three different substrates. Of the three, UvrA was found to bind to the (+)-*trans-anti*-MC-N^2-dG 50-mer with the greatest affinity, whereas UvrA binding to the C8-AP-dG adducted DNA occurred with the lowest affinity. The binding of UvrA to (−)-*cis-anti*-BP-N^2-dG DNA was greater than to the C8-AP-dG adducted DNA. These results are in good agreement with previously reported K_d value using fluorescence spectroscopy (*15*) and suggests that UvrA binding is sensitive to conformational changes induced by structurally different bulky adducts. Furthermore, these results suggest that the C8-AP-dG may not be a good substrate for UvrABC endonuclease. However, the equilibrium dissociation constant (K_d) of UvrA to a nondamaged 50-mer of the same sequence has been determined to be about 1.7 μM under identical experimental condition, showing a 2 orders of magnitude lower UvrA binding affinity to nondamaged substrate. We have noted such weak nonspecific binding to nondamaged DNA in other studies as well (*25*).

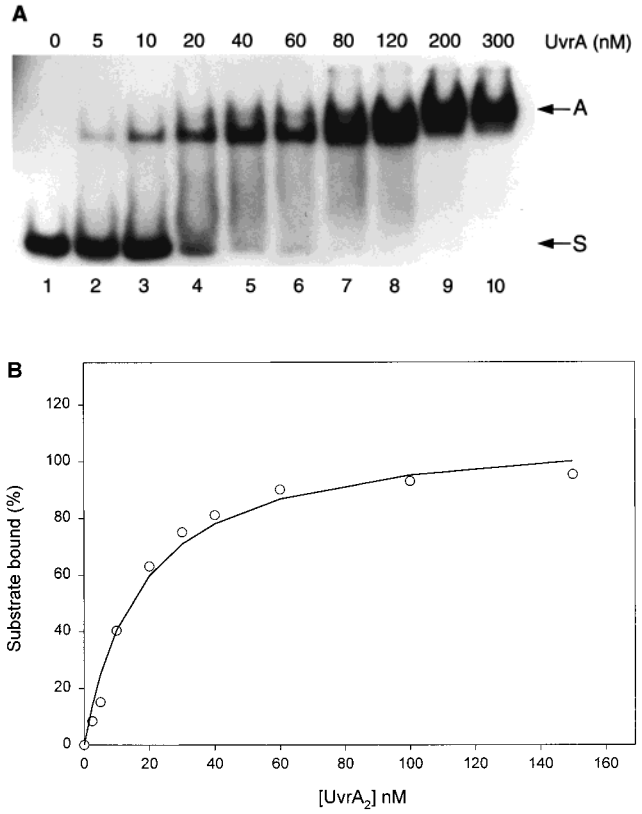

FIGURE 2: Electrophoretic mobility shift assays. Panel A: Typical gel mobility shift analysis of UvrA with 50-mer substrate containing (+)-*trans-anti*-MC-N^2-dG. The substrates, 5′ end-labeled (1 nM), were incubated at 37 °C for 15 min with UvrA at the concentrations specified, in the presence of 1 mM ATP and 10 mM $MgCl_2$ and electrophoresed on 4% native polyacrylamide gels. The dried gels were exposed to a PhosphorImager screen. Panel A shows the UvrA−DNA complex formed, in which S is the substrate free of proteins. Mobility shift assays were carried out in a similar manner for substrates containing (−)-*cis-anti*-BP-N^2-dG or C8-AP-dG lesion. Panel B: Binding isotherm of UvrA with 5-MeCDE-adducted substrate. The concentration was expressed for UvrA dimers unless otherwise specified. The binding isotherms for substrates containing (+)-*trans-anti*-MC-N^2-dG, C8-AP-dG, and (−)-*cis-anti*-BP-N^2-dG were derived from three independent experiments, and the curve shows the best fit of the calculated binding isotherms to the experimental data (for details see ref *15*).

Even so, we wish to point out that the UvrA binding affinity is not always indicative of incision efficiency (*25*, *39*). Cooperative interaction with other repair subunits may be important to achieve high incision specificity (*14*).

(b) Formation of the Preincision Complex with $UvrA_2$ and UvrB. Even though UvrA binding affinities with the three damaged substrates were significantly different, UvrA binding to damaged sites alone cannot adequately explain damage recognition. To examine the role of UvrB in damage recognition, we analyzed the interaction of UvrA in the presence of excess UvrB with the three DNA adducts (Figure 3, panels A−C) by the gel mobility shift assay. The retarded bands included $UvrA_2B$−DNA and the UvrB−DNA complexes (*25*, *39*). The formation of $UvrA_2B$ and UvrB−DNA complexes was quantitated as a function of UvrA concentration, and the combined data from three sets of experiments (including the ones shown in panels A−C) are shown in Figure 3, panel D. The relative amounts of UvrB−DNA complex formed with these substrates were different. The (+)-*trans-anti*-MC-N^2-dG showed the highest amount of substrate engaged in the UvrB−DNA complex followed by (−)-*cis-anti*-BP-N^2-dG and C8-AP-dG (Figure 3, panel D). As shown in Figure 3, panel D, in each case with increasing concentration of UvrA, the proportion of UvrB−DNA complex initially increased, reached a plateau, and then decreased as the proportion of $UvrA_2B$−DNA complex increased. It is interesting that, at a 2 nM UvrA concentration, the C8-AP-dG-modified DNA showed higher amounts of $UvrA_2B$ complexes with the UvrA and UvrB proteins in comparison to DNA containing the two N^2-dG adducts. However, at a 10 nM UvrA concentration, (+)-*trans-anti*-MC-N^2-dG, (−)-*cis-anti*-BP-N^2-dG, and C8-AP-dG adducts showed 39, 25, and 18% of the substrate bound to UvrB, respectively. These results indicate a clear difference in the stability and relative amounts of UvrB−DNA complexes formed with structurally different lesions, which may be an important factor in determining the incision efficiency.

Table 1: Equilibrium Dissociation Constants for the Binding of UvrA to Adducted DNA at 37 °C[a]

substrate	$K_{d,obs}$ (nM)
C8-AP-dG	28 ± 1
(−)-*cis-anti*-BP-N^2-dG	21 ± 2
(+)-*trans-anti*-MC-N^2-dG	17 ± 2

[a] The data represent the mean ± standard deviation of three independent experiments. The dissociation constants were determined by UvrA dimers unless otherwise indicated. Analysis of $K_{d,obs}$ values for each adduct by an unpaired student's t -test with GraphPad InStat tm indicated that binding of UvrA dimer to the C8-AP-dG DNA as compared to the (−)-*cis-anti*-BP-N^2-dG DNA is significantly different ($P = 0.019$) while the difference in binding between the C8-AP-dG DNA and (+)-*trans-anti*-MC-N^2-dG DNA is even more significant ($P = 0.0007$).

UvrABC Incision of DNA Substrates. To examine the incisions near the (+)-*trans-anti*-MC-N^2-dG, (−)-*cis-anti*-BP-N^2-dG, and C8-AP-dG adduct sites by UvrABC nuclease and to determine if these incisions correlate with the specific binding of UvrA and UvrB, 5′ and 3′ end-labeled substrates (1 nM) along with undamaged DNA, were incubated with optimal amounts of UvrA, UvrB, and UvrC proteins. The reaction products were separated on denaturing polyacrylamide gels. As shown in Figure 4, panel A, 5′ incisions occurred at the eighth phosphodiester bond from the modified base. Figure 4, panel B, represents the time course of the 5′ incision reaction determined from three independent experiments. The incision efficiency was the highest for DNA containing (+)-*trans-anti*-MC-N^2-dG, whereas C8-AP-dG was incised least efficiently. Specifically, after 30 min, 42% of (+)-*trans-anti*-MC-N^2-dG, 40% (−)-*cis-anti*-BP-N^2-dG, and 20% of C8-AP-dG modified oligonucleotides were incised. In contrast, the 3′ incision reaction displayed different incision patterns among these damaged substrates (Figure 4, panel C). UvrABC induced incisions predominantly at the fifth phosphate, 3′ to the modified site in all three cases. Incisions at the sixth and seventh phosphodiester bonds were also observed in the case of (+)-*trans-anti*-MC-N^2-dG and (−)-*cis-anti*-BP-N^2-dG adducts, whereas products (<10%) corresponding to incisions at the fourth and sixth phosphates were found for C8-AP-dG-modified DNA. The graphical representation of the time course of 3′ incision (Figure 4, panel D) shows the mean of at least three independent determinations, with the standard deviations. Quantitative determinations of 3′ incision products also

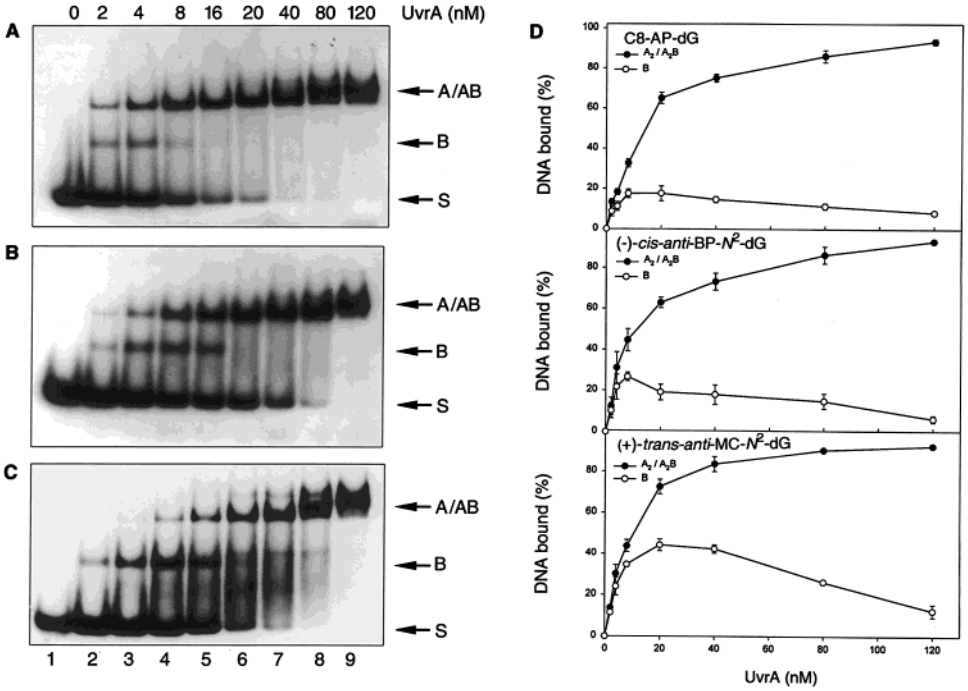

FIGURE 3: Binding of UvrA and UvrB with C8-AP-dG- (panel A), (−)-*cis-anti*-BP-N^2-dG- (panel B), and (+)-*trans-anti*-MC-N^2-dG-modified (panel C) oligonucleotide duplexes. Gel mobility shift analysis of adducted substrates. The concentrations of UvrA ranged from 0 to 120 nM, while the UvrB concentration was held constant at 200 nM. UvrA and UvrB were incubated at 37 °C for 30 min with 5′ end-labeled substrates (1 nM). Reactions were analyzed on 4% nondenaturing polyacrylamide gels and exposed to a PhosphorImager screen. Labels A/AB and B represent the formation of $UvrA_2B$, $UvrA_2$, and UvrB−DNA complexes with substrates respectively, and S denotes the substrates free of proteins. Panel D: UvrA/UvrB binding isotherms for C8-AP-dG, (−)-*cis-anti*-BP-N^2-dG, and (+)-*trans-anti*-MC-N^2-dG containing substrates determined from quantitative analyses of gel shift results. Bars indicate the standard deviation of three independent experiments including the ones shown in panels A−C. Open circles indicate the binding with UvrB alone, whereas closed circles represent binding with $UvrA_2/A_2B/B$.

indicated a high incision rate for the (+)-*trans-anti*-MC-N^2-dG, followed by (−)-*cis-anti*-BP-N^2-dG, while the C8-AP-dG adduct was incised least efficiently. Table 2 provides a summary of the initial rates and extent of 5′ and 3′ incisions derived from the above experiments. Both the 5′ and 3′ incision results showed consistently that C8-AP-dG was incised less efficiently than the (+)-*trans-anti*-MC-N^2-dG and (−)-*cis-anti*-BP-N^2-dG adducts in the identical sequence context.

UvrABC Incision of Substrates Containing a Bubble or a Deleted Base Opposite the Lesion. Recent studies indicated that $UvrA_2B$ takes part in the strand opening, thereby allowing UvrB to gain access and to bind directly to the DNA adduct (*22*). Results presented here indicated that UvrA is bound to C8-AP-dG with a lower affinity than the (+)-*trans-anti*-MC-N^2-dG and (−)-*cis-anti*-BP-N^2-dG adducts. To determine whether the lower binding affinity for UvrA is responsible for the poor incision efficiency, we used bubble substrates containing noncomplementary regions of 3−6 bases around the lesion (B3 and B6 in Table 3). In comparison to the normal substrate B0 (C8-AP-dG located opposite dC), opening of a DNA duplex by up to six bases (B6) around the C8-AP-dG site has a marginal effect on the incision efficiency. A reduction in the incision rate was observed for substrates containing unpaired strands up to three bases. 3′ Incisions occurred predominantly at the fifth phosphodiester bond for B3 like B0 and at the fourth phosphate for B6 (Figure 5, panel A).

1-NP induces frame shift mutations at a high frequency (*40*−*42*). A major fraction of 1-NP-induced frame shifts involves single base deletions. It was also shown that in duplex form the central DNA sequence used in the current investigation is thermodynamically most stable when there is no base opposite C8-AP-dG (*33*). These observations led us to investigate the repair of C8-AP-dG when cytosine opposite the modified guanine was missing (Δ*C* in Table 3). It is noteworthy that the nucleotide excision repair activity of the substrate containing this deletion was reduced by a factor of ∼2 in comparison to the substrate with a full, normal complementary strand (Figure 5, panel B; Table 3).

DISCUSSION

The UvrABC nuclease system removes DNA damage in three steps involving damage recognition, unwinding of DNA around the lesion, and dual incision by two separate endonucleases (*4*). The remarkable ability of UvrABC to recognize and eliminate structurally different lesions prompted us to address damage recognition and the stability of DNA repair intermediates and also to look into a possible relationship of these factors to overall damage removal. Three different lesions with different structural characteristics, but in the same sequence context, were selected to probe differences in interactions with the UvrABC components. We present evidence that UvrABC incises the minor groove (+)-*trans-anti*-MC-N^2-dG and that the mode of 5′ and 3′ incision is similar to the pattern observed in the case of the (−)-*cis-anti*-BP-N^2-dG adduct (*25*) that has a base-displaced adduct conformation. Understanding how DNA repair proteins in *E. coli* recognize and remove these toxic and mutagenic lesions (*42*−*45*) in DNA has profound biological significance.

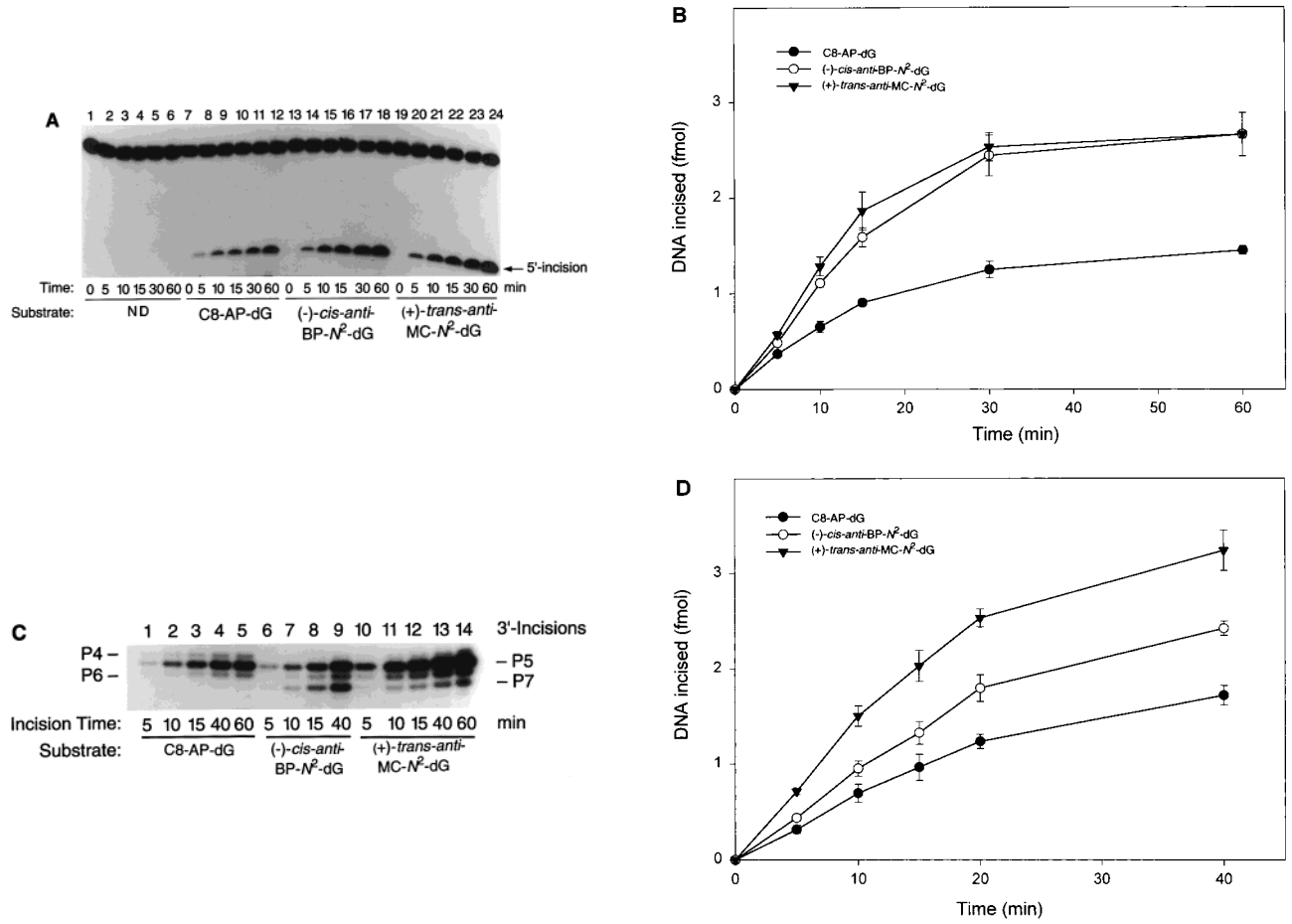

FIGURE 4: Incision of 5′ and 3′ end-labeled 50 base pair-damaged DNA duplexes by UvrABC nucleases. Panel A: incision time course for undamaged DNA (ND) and DNA containing C8-AP-dG, (−)-*cis-anti*-BP-N^2-dG, and (+)-*trans-anti*-MC-N^2-dG lesions. Substrates (1 nM) were incubated with UvrA (30 nM), UvrB (80 nM), and UvrC (150 nM) at 37 °C for the specified time period. The incised products were analyzed on 8% denaturing polyacrylamide gels. Panel B: The graph represents quantitative analysis of three independent 5′-incision experiments for each substrate as shown in panel A, and the bars indicate standard deviation derived from all three experiments. Panel C: Incision of 3′ end-labeled substrates containing C8-AP-dG, (−)-*cis-anti*-BP-N^2-dG, and (+)-*trans-anti*-MC-N^2-dG lesions. Incisions were performed as described above. The products were analyzed on a 12% denaturing polyacrylamide gel. P4, P5, P6, and P7 indicate fourth, fifth, sixth, and seventh phosphodiester bond 3′ toward the modified guanine. Panel D: 3′ Incision time course shown graphically represents the mean of at least three independent determinations with standard deviations.

Table 2: Initial Rate and Extent of 5′ and 3′ Incisions[a]

	5′ incisions		3′ incisions	
substrate	initial rate fmol/min	extent at 15 min fmol	initial rate fmol/min	extent at 15 min fmol
C8-AP-dG	0.07 ± 0.00	0.90 ± 0.01	0.06 ± 0.00	0.97 ± 0.14
(−)-*cis-anti*-BP-N^2-dG	0.11 ± 0.01	1.59 ± 0.10	0.09 ± 0.00	1.33 ± 0.12
(+)-*trans-anti*-MC-N^2-dG	0.10 ± 0.01	1.86 ± 0.20	0.14 ± 0.01	2.03 ± 0.16

[a] The data represent the mean + sd of three independent experiments. The incision rate is the slope of the line obtained from unweighted linear regression derived from values obtained at 5, 10, and 15 min, respectively.

It is widely accepted that UvrA plays an important role in damage recognition (*14*). The nature of the specific binding of UvrA to the damaged DNA can reveal the mechanism underlying damage recognition. On the basis of quantitative gel retardation assays, we found that UvrA binds with different affinities to the structurally different lesions used in this study, while nonspecific binding to nondamaged substrates is very weak. Interestingly, the incision efficiencies appear to be correlated to the binding constants. Our data are in accord with similar observations made by Visse et al. (*38*). In a prior study (*25*), a correlation between UvrA binding and incision efficiencies in the case of four stereoisomeric *anti*-BP-N^2-dG adducts, including the (−)-*cis-anti*-BP-N^2-dG lesion, was not observed. However, employing structurally different, rather than structurally similar, stereoisomeric sets of adducts (*25*), our results in the current investigation suggest that UvrA can detect lesion-dependent conformational changes in the DNA duplex and that the binding affinity of UvrA to these lesion can also represent an important factor in determining the incision efficiency.

The binding of UvrB to the damaged site adds a second level of discrimination to damage recognition (*14*, *22*, *23*). UvrB is believed to contact an adducted base through a hydrophobic interaction (*23*, *39*, *46*). Snowden and Van Houten (*27*) demonstrated that UvrB−DNA complex formation on an abasic site was the rate-limiting factor in the overall incision reaction. A sequence-dependent isomerization, or change in conformation of the UvrB−DNA complex

Table 3: Initial Rate for Bubble and Deletion Substrates[a]

	Substrate	Initial rate (fmol/min)
5'-incision 3'-incision ^{32}P-GACTACGTACTGTTACGGCTCCATC**G**CTACCGCAATCAGGCCAGATCTGC CTGATGCATGACAATGCCGAGGTAGCGATGGCGTTAGTCCGGTCTAGACG	B0	0.066 ± 0.002
^{32}P-GACTACGTACTGTTACGGCTCCA**T**^{C}**G**CTACCGCAATCAGGCCAGATCTGC CTGATGCATGACAATGCCGAGGTCTTGATGGCGTTAGTCCGGTCTAGACG	B3	0.048 ± 0.003
^{32}P-GACTACGTACTGTTACGGCTCCA**T**^{CG}**C**$^{T}_{A}$CCGCAATCAGGCCAGATCTGC CTGATGCATGACAATGCCGAGGTCTTTTCGGCGTTAGTCCGGTCTAGACG	B6	0.065 ± 0.003
^{32}P-GACTACGTACTGTTACGGCTCCATCCTACCGCAATCAGGCCAGATCTGC CTGATGCATGACAATGCCGAGGTAGGATGGCGTTAGTCCGGTCTAGACG	ΔC	0.037 ± 0.006

[a] The bold G with an asterisk in the sequence represents the base containing the C8-AP adduct. The data represent the mean ± sd of the three independent experiments. The incision rate is the slope of the line obtained from unweighted linear regression.

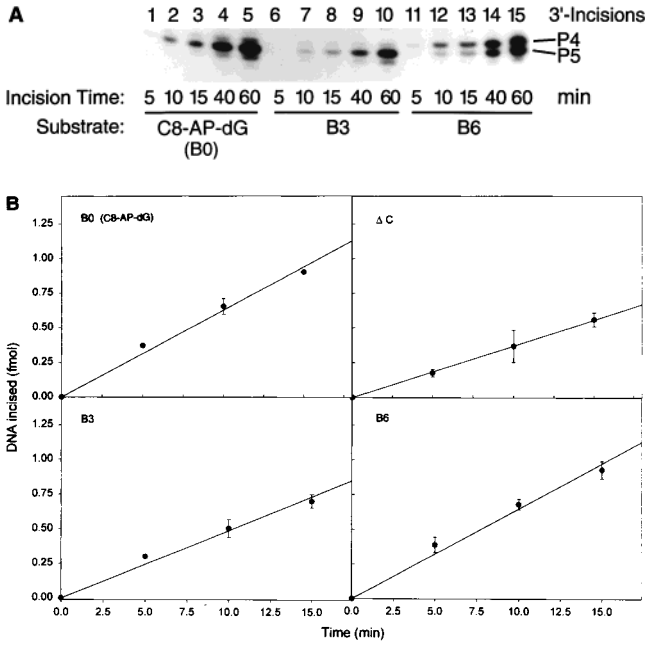

FIGURE 5: UvrABC incision of bubble and deletion substrates containing C8-AP-dG. Panel A: Incision time course of 3′ end-labeled bubble substrates with three and six mismatches (B3 and B6) in the bottom strand, in comparison to the normal substrate (B0) (left panel). P4 and P5 indicate the fourth and fifth phosphodiester bond, respectively. Panel B: Initial rates of incision for B0, B3, B6, and the substrate containing the deletion (Δ*C*). The data represent the mean of three independent experiments with standard deviations.

after the release of $UvrA_2$, is also considered to be an important factor in modulating NER efficiency (*11*). Therefore, we quantitated the amount of UvrB−DNA complex formed with each of the three lesions. We found that the (+)-*trans-anti*-MC-N^2-dG adduct-containing DNA duplex, which forms a UvrB complex with the greatest affinity, is also incised with the highest efficiency. The lower incision rate of the C8-AP-dG-containing DNA could be due to the poor interaction of UvrB with the adducted site. The UvrB−DNA complexes form with 50% lower affinities in the case of the (−)-*cis-anti*-BP-N^2-dG adduct than in the case of the (+)-*trans-anti*-MC-N^2-dG adduct; however, both of these lesions were incised on the 5′ side of the lesions with equal efficiencies by UvrABC (Figure 4, panel B). This observation suggests that the ultimate damage recognition step leading to the removal of the lesion may be governed by the formation of the UvrBC−DNA complex. This is also supported by evidence that the 3′ incision triggered by the interaction of the carboxyl terminus of UvrB with UvrC (*47*) is the rate-limiting step (*48*, *49*).

Although UvrABC incised the eighth phosphate 5′, and predominantly the fifth phosphate 3′ to all three lesions (*25*), minor products resulting from the 3′ incision of the sixth and seventh phosphates were also seen in the case of the (−)-*cis-anti*-BP-N^2-dG and the (+)-*trans-anti*-MC-N^2-dG-containing substrates. Interestingly, C8-AP-dG adducted DNA showed cutting at the fourth and the sixth phosphates in addition to the fifth phosphate. The N-terminal portion of UvrC is believed to perform the rate-limiting 3′ incision, whereas the C-terminal portion of UvrC cleaves on the 5′ side of the modified site, once the 3′ incision has occurred (*26*). The pyrenyl moiety of the C8-AP-dG, like that of the (−)-*cis-anti*-BP-N^2-dG adduct, is positioned at an intercalated site in DNA with the modified dG and partner dC residue on the complementary strand displaced into the major groove (*32*, *37*). An important difference between the two, however, is that the major intercalated conformation of (−)-*cis-anti*-BP-N^2-dG remains in equilibrium with a minor conformer [reviewed in Geacintov et al. (*50*)], whereas the C8-AP-dG is characterized by a single, base-displaced intercalative conformation (*37*). It is conceivable that the recognition of the minor conformer of the (−)-*cis-anti*-BP-N^2-dG is more favorable than the recognition of the major intercalated conformer.

Among the three different lesions studied in this work, the C8-guanine adduct formed by 1-NP is recognized and repaired with the lowest efficiency by UvrABC. We used bubble substrates containing non-hydrogen bonded regions around the lesion to determine whether bypassing the first level of damage recognition can enhance the incision efficiency. $UvrA_2B$, by virtue of its limited helicase activity, inserts itself into the DNA duplex in search of an abnormality and directs UvrB to the damaged site, thereby allowing UvrB to form a stable preincision complex (*22*). Our data, using six-base bubble substrates containing C8-AP-dG, showed marginal differences in the incision rates in comparison to substrates without a bubble structure (B0), whereas a three-base bubble substrate exhibited a reduction in the incision rate. The 3′ incision was predominant at the fourth phosphate in the bubble substrate (B6).

We examined the effect of deletion of the complementary base opposite the C8-AP-dG on adduct excision by UvrABC. This structure models a promutagenic intermediate of a single-base deletion, which is one of the major types of mutations induced by C8-AP-dG (*40*−*42*). The modified duplex containing a single deleted base in the complementary strand is thermodynamically much more stable than the normal full duplex with a C or any other base opposite C8-AP-dG (*33*). Interestingly, the single-base deletion of C across the modified base showed a 50% reduction in the incision efficiency suggesting that the C deletion alters the conformation of the adduct in such a way that UvrABC cannot detect the lesion as efficiently. NMR analysis of an 11-mer containing C8-AP-dG showed an intrahelical insertion of the aromatic ring into the DNA helix, leading to a rupture of base pairing at the modified site and the displacement of modified guanine and the complementary cytosine in the major groove (*37*). Deletion of C opposite C8-AP-dG may result in a less distorted intercalated structure, since only one base rather than two might be displaced into the major groove of the single deletion duplex. This may lead to a decreased recognition and incision by the UvrABC nuclease system. Thus, the conformation resulting from the displacement of a single base is not as effective as the displacement of both bases in facilitating the assembly of the functional incision complexes at the site of the damage. The conformation of the (+)-*cis*-*anti*-BP-N^2-dG adducts in a full duplex (*51*) is similar to that of the (−)-*cis*-*anti*-BP-N^2-dG adducts (*32*) studied in this work. In the (+)-cis adduct, the bulky pyrenyl residue is intercalated and the modified guanine and partner cytosine residues are displaced into the minor and major grooves, respectively. When the partner cytosine is deleted, the structural features of the (+)-cis adduct do not change significantly, with only the modified guanine displaced into the minor groove (*52*). While the structure of the (−)-*cis*-*anti*-BP-N^2-dG adduct deletion duplex has not been investigated, its structure, minus the cytosine opposite the lesion site, would also be similar to that of the full duplex (*50*). Hess et al. (*53*) found, however, that the excision of the (−)-*cis*-*anti*-BP-N^2-dG adducts is almost completely abolished in the case of the deletion duplex, whereas the same lesion in the full duplex is efficiently excised by human nucleotide excision repair proteins in a cell-free DNA repair assay. Thus, our observation of the lower excision efficiency of the C8-AP-dG adduct in the Δ*C* duplex, is consistent with the trend observed by Hess et al. (*66*), although the structure of the adduct is different.

The relative rates of incision of the four stereoisomeric lesions (−)-*cis*-, (+)-*trans*-, (+)-*cis*-, and (−)-trans-*anti*-BP-N^2-dG, all in the same sequence context as studied in this work, have been previously investigated (*25*). The two *trans* adducts reside in the minor groove with all base pairs intact, while the conformations of the two *cis* adducts are of the base-displaced intercalation type [summarized in Geacintov et al. (*50*)]. The relative incision rates by the UvrABC nuclease do not seem to be correlated with the absolute *R* or *S* configurations at the C10 BP-N^2-dG linkage site. However, for the pair of adducts derived from either the (+)- or the (−)-enantiomer of *anti*-BPDE, the base-displaced *cis* adducts are incised more efficiently than the minor groove *trans* adducts. Furthermore, within each class of conformations (base-displaced or minor groove), the DNA adducts derived from (−)-*anti*-BPDE are less efficiently incised by factors of ∼2 than those derived from (+)-*anti*-BPDE. Thus, the absolute configurations of the substituents about the 7,8,9-carbon atoms of the bulky, saturated BP ring appears to be linked with incision efficiencies. In the case of NER by human repair proteins, the two base-displaced *cis* adducts in the same sequence context were excised with efficiencies 8−10 times greater than the two minor groove adducts (*53*).

In this work, we compared the relative excision rates by UvrABC of the 4*S* (+)-*trans*-*anti*-MC-N^2-dG adduct [most likely a minor groove adduct (*31*, *46*)] and the two base displaced intercalated lesions, the 10*S* (−)-*cis*-*anti*-BP-N^2-dG and the C8-AP-dG adducts. Interestingly, the C8-AP-dG lesion is excised less efficiently than the 10*S* (−)-*cis*-*anti*-BP-N^2-dG lesion, even though both have similar base-displaced intercalative conformations, with both the modified dG and partner strand dC residues displaced into the minor groove. We speculate that the bulky benzylic ring in the (−)-*cis*-*anti*-BP-N^2-dG adduct causes a greater local disturbance of the local DNA structure that is sensed by the UvrABC proteins. Another difference between the two base-displaced intercalated adducts is the syn glycosidic torsion angle adopted by the C8-AP-dG adduct, while in the (−)-*cis*-*anti*-BP-N^2-dG adduct the glycosidic torsion angle is anti (*32*, *37*). Furthermore, the orientation of the long axis of the pyrenyl residues relative to the orientation of the flanking dG·dC base pairs is different in the two adducts, which is parallel in the C8-AP-dG adduct and orthogonal in the (−)-*cis*-*anti*-BP-N^2-dG adduct (*37*). It is not clear at this point how each of these effects contributes to the recognition by UvrABC proteins and the incision efficiencies.

Among the three different lesions studied in this work, the (+)-*trans*-*anti*-MC-N^2-dG adduct exhibits the highest UvrA binding affinity (Table 1) and the highest rate of 3′-incision (Figure 4, panel D). The (+)-*trans*-*anti*-MC-N^2-dG adduct in double-stranded DNA is significantly distorted by bending as shown by its reduced electrophoretic mobility (*31*). In the case of the (−)-*trans*-*anti*-MC-N^2-dG lesion in a duplex of identical sequence context, the 5-methyl group causes significant distortions in the normal B-DNA structure, even though the adduct is positioned in the minor groove (*52*). Similar distortions in the case of the (+)-*trans*-*anti*-MC-N^2-dG adduct studied here could account for the observed enhanced efficiency of recognition and processing of this adduct by UvrABC protein.

CONCLUSIONS

Using a defined substrate containing structurally different bulky DNA adducts all within the same sequence context, we found that all three levels of damage discrimination including binding of $UvrA_2$, formation of preincision, and incision complexes are important in modulating incision efficiency. Studies from many laboratories showed that the repair process centers on UvrB as this subunit contacts the modified base and most of the components in NER (*21*−*23*). Any of these components might cause a conformational change in UvrB. The formation of the incision complex is dependent on this conformational change, which ultimately determines the repair efficiency. Our study shows that UvrABC nuclease can discriminate substrates that do not have a partner base in the complementary strand, opposite

the lesion. An analogous effect was reported in the case of the excision of similar adducts by human NER proteins (*53*).

REFERENCES

1. Van Houten, B. (1990) *Microbiol. Rev. 54*, 18−51.
2. Lin, J. J., Sancar, A. (1992) *Mol. Microbiol. 6*, 2219−2224.
3. Sancar, A. (1994) *Science 266*, 1954−1956.
4. Sancar, A., Rupp, D. W. (1983) *Cell 33*, 249−260.
5. Van Houten, B., Gamper, H., Holbrook, S. R., Hearst, J. E., Sancar, A. (1986) *Proc. Natl. Acad. Sci. U.S.A. 83*, 8077−8083.
6. Gao, S., Drouin, R., Chen, R., Holmquist, G. P. (1994) *Science 263*, 1438−1440.
7. Tornaletti, S., Pfeifer, G. P. (1994) *Science 263*, 1436−1438.
8. Jones, B., Yeung, A. T. (1988) *Proc. Natl. Acad. Sci. U.S.A. 85*, 8410−8414.
9. Seeberg, E., Fuchs, R. (1990) *Proc. Natl. Acad. Sci. U.S.A. 87*, 191−194.
10. Ramaswamy, M., Yeung, A. T. (1994) *J. Biol. Chem. 269*, 485−492.
11. Delagoutte, E., Bertrand-Burggraf, E., Dunand, J., Fuchs, R. P. P. (1997) *J. Mol. Biol. 266*, 703−710.
12. Mekhovich, O., Tang, M., Romano, L. J. (1998) *Biochemistry 37*, 571−579.
13. Sancar, A., Sancar, G. (1988) *Annu. Rev. Biochem. 57*, 29−67.
14. Lloyd, R. S., Van Houten, B. (1995) *DNA Repair Mechanisms: Impact on Human Diseases and Cancer*, Chapter 2, R. G. Landes Company, Biochemical Publishers, Austin.
15. Zou, Y., Basset, H., Walker, R., Bishop, A., Amin, S., Geacintov, N. E., Van Houten, B. (1998) *J. Mol. Biol. 281*, 107−119.
16. Oh, E. Y., Claasen, L., Thiagalingam, S., Mazur, S., Grossman, L. (1989*) Nucleic Acids Res. 17*, 4145−4159.
17. Orren, D. K., Sancar, A. (1990) *J. Biol. Chem. 265*, 15796−15803.
18. Oh, E. Y., Grossman, L. (1987) *Proc. Natl. Acad. Sci. U.S.A. 84*, 3638−3642.
19. Oh, E. Y., Grossman, L. (1989) *J. Biol. Chem. 264*, 1336−1343.
20. Shi, A., Thresher, R., Sancar, A., Griffith, J. (1992) *J. Mol. Biol. 26*, 425−432.
21. Sancar, A., Tang, M.-S. (1993) *Photochem. Photobiol. 57*, 905−927.
22. Zou, Y., Van Houten, B. (1999) *EMBO J. 18(17)*, 4889−4901.
23. Hsu, D. S., Kim, S.-T., Sun, Q., Sancar, A. (1995) *J. Biol. Chem. 270*, 8319−8327.
24. Lin, J. J., Phillips, A. M., Hearst, J. E., Sancar, A. (1992) *J. Biol. Chem. 267*, 17693−17700.
25. Zou, Y., Liu, T.-M., Geacintov, N. E., Van Houten, B. (1995) *Biochemistry 34*, 13582−13593.
26. Verhoeven, E. E. A., van Kesteren, M., Moolenaar, G. F., Visse, R., and Goosen, N. (2000) *J Biol. Chem. 275*, 5120−5123.
27. Snowden, A., Van Houten, B. (1991) *J. Mol. Biol. 220*, 19−33.
28. Orren, D. K., Selby, C. P., Hearst, J. E., Sancar, A. (1992) *J. Biol. Chem. 267*, 780−788.
29. Heflich, R. H., Howard, P. C., Beland, F. A. (1985) *Mutat. Res. 149*, 25−32.
30. Stanton, C. A., Chow, F. L., Phillips, D. H., Grores, R. C., Martin, C.-N. (1985) *Carcinogenesis 6*, 535−538.
31. Xu, R., Dwarakanath, S., Cosman, M., Amin, S., and Geacintov, N. E. (1996) *Carcinogenesis 17*, 2035−2042.
32. Cosman, M., Hingerty, B. E., Luneva, N., Amin, S., Geacintov, N. E., Broyde, S., Patel, D. J. (1996) *Biochemistry 35*, 9850−9863.
33. Nolan, S. J., McNulty, J. M., Krishnasamy, R., McGregor, W. G., and Basu, A. K. (1999) *Biochemistry 38*, 14056−14062.
34. Amin, S., Hue, K., Melikian, A. A., Leszcynska, J. M., Hecht, S. S. (1985*) Cancer Res. 45*, 6406−6442.
35. Miroux, B., Walker, J. E. (1996) *J. Mol. Biol. 260*, 289−298.
36. Sancar, A., Thomas, D. C., Van Houten, B., Husain, I., and Levy, M. (1987) in *DNA Repair, A Laboratory Manual of Research Procedures* (Friedberg, E. C., and Hanawalt, P. C., Eds.) Vol 3, Chapter 24, pp 479−508, Mercel Deckker, New York.
37. Mao, B., Vyas, R. R., Hingerty, B. E., Broyde, S., Basu, A. K., Patel, D. J. (1996) *Biochemistry 35*, 12659−12670.
38. Visse, B., de Ruijter, M., Moolenaar, G. F., and van de Putte, P. (1992) *J. Biol. Chem. 267*, 6736−6742.
39. Van Houten, B., Snowden, A. (1993) *BioEssays 15*, 51−59.
40. Stanton, C. A., Garner, R. C., and Martin, C. N. (1988) *Carcinogenesis 9*, 1153−1157.
41. Melchior, W. B., Jr., Marques, M. M., and Beland, F. A. (1994) *Carcinogenesis 15*, 889−899.
42. Malia, S. A., and Basu, A. K. (1995) *Biochemistry 34*, 96−104.
43. Hecht, S. S., Ronai, Z. A., Dolan, L., Desai, D., and Amin, S. (1998) *Carcinogenesis 19*, 157−160.
44. Shukla, R., Jelinsky, S., Liu, T., Geacintov, N. E., and Loechler, E. L. (1997) *Biochemistry 36*, 13263−13269.
45. Fernandes, A., Liu, T., Amin, S., Geacintov, N. E., Grollman, A. P., and Moriya, M. (1998) *Biochemistry 37*, 10164−10172.
46. Theis, K. K., Chen, P. J., Skorvaga, M., Van Houten, B., and Kisker, C. (1999) *EMBO J. 18*, 6899−6907.
47. Moolenaar, G. F., Franken, K. L., Dijkstra, D. M., Thomas-Oates, J. E., Visse, R., van de Putte, P., Goosen, N. (1995) *J. Biol. Chem. 270*, 30508−30515.
48. Zou, Y., Walker, R., Bassett, H., Geacintov, N. E., and Van Houten, B. (1997) *J. Biol. Chem. 272*, 4820−4827.
49. Mekhovich, O., Tang, M.-S., and Romano, L. J. (1998) *Biochemistry 37*, 571−579.
50. Geacintov, N. E., Cosman, M., Hingerty, B. E., Amin, S., Broyde, S., and Patel, D. J. (1997) *Chem. Res. Toxicol. 10*, 111−146.
51. Cosman, M., de los Santos, C., Fiala, R., Hingerty, B. E., Ibanez, V., Luna, E., Harvey, R. G., Geacintov, N. E., Broyde, S., and Patel, D. (1993) *Biochemistry 32*, 4145−4155.
52. Cosman, M., Fiala, R., Hingerty, B. E., Amin, S., Geacintov, N. E., Broyde, S., and Patel, D. J. (1995) *Biochemistry 33*, 11518−11527.
53. Hess, M. T., Gunz, D., Luneva, N., Geacintov, N. E., and Naegeli, H. (1997) *Mol. Cell. Biol. 17*, 7069−7076.

BI0013187